Biomech Model Mechanobiol (2016) 15:97–109
DOI 10.1007/s10237-015-0689-6

ORIGINAL PAPER

Elasticity–density and viscoelasticity–density relationships at the tibia mid-diaphysis assessed from resonant ultrasound spectroscopy measurements

Simon Bernard[1] · **Joannes Schneider**[2] · **Peter Varga**[2] · **Pascal Laugier**[1] · **Kay Raum**[2] · **Quentin Grimal**[1]

Received: 22 December 2014 / Accepted: 30 May 2015 / Published online: 13 June 2015

Abstract Cortical bone tissue is an anisotropic material characterized by typically five independent elastic coefficients (for transverse isotropy) governing shear and longitudinal deformations in the different anatomical directions. It is well established that the Young's modulus in the direction of the bone axis of long bones has a strong relationship with mass density. It is not clear, however, whether relationships of similar strength exist for the other elastic coefficients, for they have seldom been investigated, and the results available in the literature are contradictory. The objectives of the present work were to document the anisotropic elastic properties of cortical bone at the tibia mid-diaphysis and to elucidate their relationships with mass density. Resonant ultrasound spectroscopy (RUS) was used to measure the transverse isotropic stiffness tensor of 55 specimens from 19 donors. Except for Poisson's ratios and the non-diagonal stiffness coefficient, strong linear correlations between the different elastic coefficients ($0.7 < r^2 < 0.99$) and between these coefficients and density ($0.79 < r^2 < 0.89$) were found. Comparison with previously published data from femur specimens suggested that the strong correlations evidenced in this study may not only be valid for the mid-tibia. RUS also measures the viscous part of the stiffness tensor. An anisotropy ratio close to two was found for damping coefficients. Damping increased as the mass density decreased. The data suggest that a relatively accurate estimation of all the mid-tibia elastic coefficients can be derived from mass density. This is of particular interest (1) to design organ-scale bone models in which elastic coefficients are mapped according to Hounsfield values from computed tomography scans as a surrogate for mass density and (2) to model ultrasound propagation at the mid-tibia, which is an important site for the in vivo assessment of bone status with axial transmission techniques.

Keywords Cortical bone · Anisotropy · Young's modulus · RUS · Axial transmission

1 Introduction

Fracture risk factors at cortical bone sites are cortical thickness, porosity and some bone quality factors of the extracellular matrix (ECM) (Zebaze et al. 2010). The latter may include mineralization and organization of the collagen fibers. Porosity and ECM properties are reflected in the mesoscale mechanical properties of the cortex material, i.e., tissue properties at the millimeter scale.

Cortical bone mechanical quality can be probed in vivo by ultrasound axial transmission technique (Foldes et al. 1995; Prevrhal et al. 2001; Sievänen et al. 2001; Talmant et al. 2010). Recent advances in these techniques open the way for the simultaneous measurement of cortical thickness and tissue elastic properties by ultrasound (Foiret et al. 2014). Axial transmission measurements are based on the propagation of ultrasound waves guided by the cortex, which involve several stiffness constants; accordingly, the technique is sensitive to the elastic anisotropy and to both shear and longitudinal elastic constants.

Electronic supplementary material The online version of this article (doi:10.1007/s10237-015-0689-6) contains supplementary material, which is available to authorized users.

✉ Quentin Grimal
quentin.grimal@upmc.fr

[1] Sorbonne Universités, UPMC Univ Paris 06, INSERM UMR-S 1146, CNRS UMR 7371, LIB 15, Rue de l'Ecole de Medecine, 75006 Paris, France

[2] Julius-Wolff-Institute & Berlin Brandenburg School for Regenerative Therapies, Charité-Universitätsmedizin Berlin, Berlin, Germany

A relevant ultrasound measurement site for axial transmission is the mid-tibia diaphysis which is relatively flat and covered by a small thickness of soft tissues. As opposed to the diaphysis of the femur, very few studies investigated the anisotropic elastic constants of the tibia. The most exhaustive study is that of Rho et al. (1995) who prepared specimens in the four quadrants of three bone slabs taken at 30, 50 and 70 % of total bone length (eight subjects). At the mid-tibia, they found that the tissue elasticity is consistent with transverse isotropy and that the ratio between the axial and transverse Young's moduli is close to 2 in average. Pooling all the specimens from the different axial and circumferential tibia regions, Rho et al. found a moderate relationship between mass density and the axial Young's modulus ($r^2 = 0.53$) and low correlations between the Young's moduli in the axial, tangential and radial directions ($r^2 < 0.2$). However, studies using specimens from the femur diaphysis suggest that cortical bone stiffness coefficients in the different anatomical directions may all have a relatively strong relationship with density and that anisotropy ratios may also be related to density (Dong and Guo 2004; Espinoza Orías et al. 2009; Granke et al. 2011). One motivation for investigating elasticity–density relationships is that bone density can be conveniently deduced from quantitative computed tomography data (Helgason et al. 2008). The relationships between different elastic coefficients and density can be used to parameterize numerical models of the skeletal system for mechanical or wave propagation analysis.

The objectives of the present work were to document the anisotropic elastic properties at the tibia mid-diaphysis, a clinically relevant site for ultrasound measurements, and to elucidate their relationships with mass density. Traditionally, ultrasound laboratory methods have been used to measure bone elastic anisotropic coefficients because these allow several coefficients to be measured on a single specimen. Here, resonant ultrasound spectroscopy (RUS) was used, which is a highly accurate method recently validated for the measurement of bone and other high damping materials (Bernard et al. 2013, 2014).

In addition to elastic coefficients, RUS yields estimates of the viscous part of the stiffness tensor. An ancillary objective of the work was to investigate the relationships between bone damping coefficients and mass density, which information is lacking in the bone literature, as far as we know.

2 Materials and methods

2.1 Specimens

A 20-mm-thick cross section was cut perpendicular to the bone axis in 19 tibiae from human cadavers at mid-diaphysis (Fig. 1). Among the 19 donors, 13 were females (ages 69–94 years, mean ± SD = 82.7 ± 8.4 years) and 6 were males (ages 70–94 years, 82.2 ± 10.1 years).

The collection and handling of the human bone tissue has been conducted in compliance with the recommendations of the World Medical Association as last revised and concluded at the 52nd General Assembly of the World Medical Association in October 2000 in Edinburgh/Scotland. The bones have been collected from human cadavers under permission of the ŒGesetz über das Leichen-, Bestattungs- und Friedhofswesen (Bestattungsgesetz) des Landes Schleswig-Holstein vom 04.02.2005, Abschnitt II, §9 (Leichenöffnung, anatomisch).

The distal part of each cross section was partially embedded in PMMA for ease of manipulation (on about 5 mm of the thickness). Up to four rectangular parallelepiped (RP), specimens were extracted from the medial tibia face (Fig. 1).

The operator manually aligned a face of each RP with the medial surface and the normal to the superior/inferior faces with the bone axis. At least two specimens were prepared for each cross section: one in the center of the medial face (centered on the H-line, see Fig. 1) and one in the extremity, centered on the $H + 2/3$ line. When the curvature of the medial face was low, one or two additional specimens could

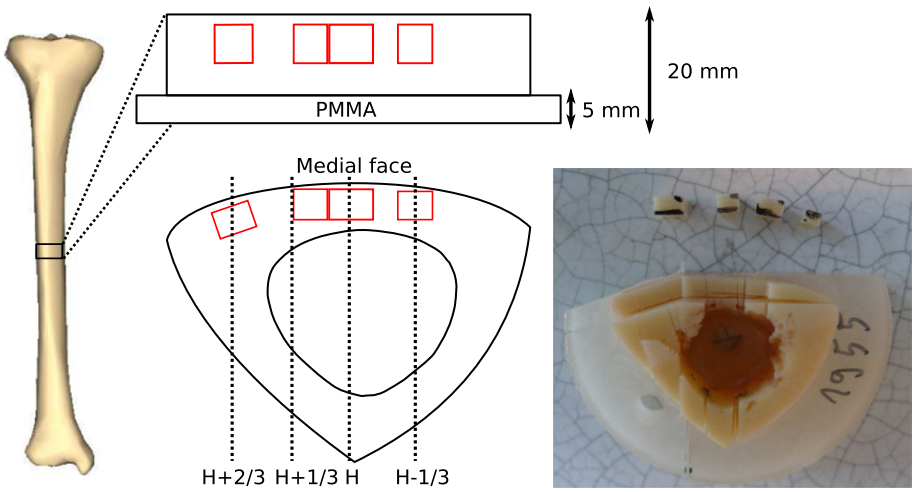

Fig. 1 Scheme and photograph of the specimens location. A cross section was harvested from the mid-diaphysis and two to four specimens extracted from the medial face at registered locations

be extracted together with the central specimen: one immediately adjacent to it, limited by the $H + 1/3$ line, and another one centered on the $H - 1/3$ line. Cutting was done using a precision linear saw (Isomet 4000, Buehler GmbH, Düsseldorf, Germany). In total, 59 RP specimens were harvested and marked so as to identify the three anatomical directions. The typical specimen size was $2 \times 3 \times 4\ \text{mm}^3$ in radial (axis 1), circumferential (axis 2) and axial (axis 3) directions, respectively. The smallest specimen was $1 \times 1.5 \times 1.7\ \text{mm}^3$, and the largest was $4.9 \times 3.8 \times 6.2\ \text{mm}^3$. Before the preparation of RP specimens, bones were stored at −20°C. The RP specimens were stored at ambient temperature in phosphate-buffered saline solution (PBS) and measured in a fully hydrated state no more than 24 h after cutting. The mass density ρ (kg.m^{-3}) of each specimen was deduced from the measured mass (precision ±0.1 mg) and dimensions (precision ±0.02 mm).

2.2 Elasticity

A transverse isotropic symmetry, associated with five independent elastic parameters, was assumed for the elastic properties of tibial cortical bone at the tissue scale (i.e., mesocale, Grimal et al. (2011)). This symmetry assumes that elasticity is isotropic in the plane orthogonal to the bone axis. It has been reported to be an accurate assumption for the elastic properties at the mid-diaphysis of the femur (Espinoza Orías et al. 2009; Granke et al. 2011) and tibia (Rho 1996). In the orthogonal reference frame defined by the faces of the RP the elasticity, or stiffness, matrix takes the form

$$\mathbb{C} = \begin{pmatrix} C_{11} & C_{12} & C_{13} & 0 & 0 & 0 \\ C_{12} & C_{11} & C_{13} & 0 & 0 & 0 \\ C_{13} & C_{13} & C_{33} & 0 & 0 & 0 \\ 0 & 0 & 0 & C_{44} & 0 & 0 \\ 0 & 0 & 0 & 0 & C_{44} & 0 \\ 0 & 0 & 0 & 0 & 0 & C_{66} \end{pmatrix}, \tag{1}$$

with $C_{12} = C_{11} - 2C_{66}$, and where the axis 3 is in the axial direction of bone and axes 1 and 2 are orthogonal to the bone axis. The stiffness coefficients are denoted C_{ij}; C_{11} and C_{33} are the longitudinal coefficients, and C_{44} and C_{66} are the shear coefficients. The inverse of the elasticity matrix writes in terms of the engineering moduli

$$\mathbb{C}^{-1} = \begin{pmatrix} 1/E_1 & \nu_{12}/E_1 & \nu_{13}/E_1 & 0 & 0 & 0 \\ \nu_{21}/E_1 & 1/E_1 & \nu_{13}/E_1 & 0 & 0 & 0 \\ \nu_{31}/E_3 & \nu_{31}/E_3 & 1/E_3 & 0 & 0 & 0 \\ 0 & 0 & 0 & 1/C_{44} & 0 & 0 \\ 0 & 0 & 0 & 0 & 1/C_{44} & 0 \\ 0 & 0 & 0 & 0 & 0 & 1/C_{66} \end{pmatrix}, \tag{2}$$

where E_i are the Young's moduli and ν_{ij} are the Poisson's ratios. The relations $\nu_{12} = \nu_{21}$ and $\nu_{13}/E_1 = \nu_{31}/E_3$ hold.

2.3 Measurement of the mesoscale stiffness tensor with resonant ultrasound spectroscopy (RUS)

Setup and signal processing methods dedicated to the RUS measurement of attenuative materials such as cortical bone, extensively described elsewhere (Bernard et al. 2013, 2014, 2015), were used in this study. Briefly, the RP specimens were placed with slight contact between a pair of shear ultrasonic transducers (V154RM, Panametrics, Waltham, MA), one acting as an emitter and the second one as a receiver. The frequency response was recorded using a vectorial network analyzer (Bode 100, Omicron Electronics GmbH, Klaus, Austria) and a broadband charge amplifier (HQA-15 M-10 T, Femto Messtechnik GmbH, Berlin, Germany). The frequency band of analysis was tuned for each specimen so as to contain the ∼20–30 first mechanical resonant frequencies of the RP (typically 150–500 kHZ). Six successive measurements on each specimen were done, with intermediate rotation of the specimens by a small angle between each measurement to vary the relative amplitudes of the excited resonant modes in order to maximize the number of detectable resonant frequencies (Fig. 2).

The spectra were fitted to a sum of M Lorentzian lineshapes (Eq. 3), each describing the behavior of a one degree-of-freedom mechanical resonator:

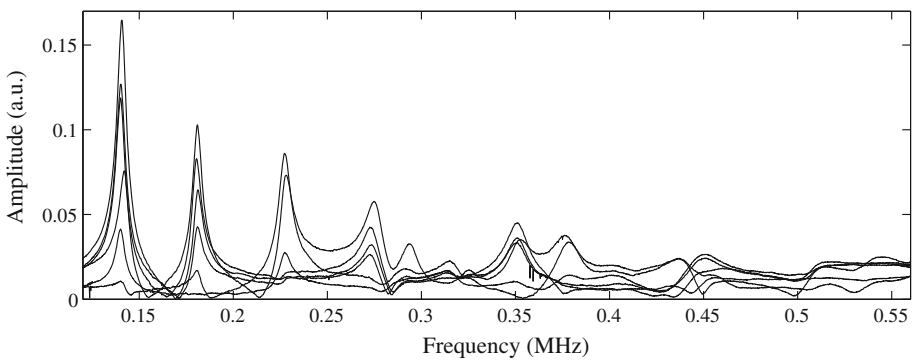

Fig. 2 Typical set of spectra measured for a cortical bone specimen. The relative amplitudes of the resonant modes vary as the specimen is rotated, allowing to detect more resonant frequencies than from a single spectrum

$$L(f) = \sum_{k=1}^{M} \frac{a_k}{(f_k^2 - f^2) + i(f_k f / Q_k)}, \tag{3}$$

with a_k the complex amplitudes, f_k the resonant frequencies and Q_k the quality factors. To estimate these parameters as well as the number of peaks M, we used a time domain estimation method based on a linear predictive filter (Lebedev 2002) followed by a frequency domain nonlinear optimization.

In RUS, the elastic properties of the RP are estimated by solving an inverse problem which consists of the comparison of the measured resonant frequencies f_n^{exp} to model-predicted frequencies f_n^{cal}. The model is that of a vibrating elastic RP with stress-free boundary conditions, which resonant frequencies are efficiently obtained with the Rayleigh–Ritz method (Migliori and Sarrao 1997). The geometry, mass density and stiffness of the specimen entirely determine the frequencies, so that the stiffness can be adjusted until the best match between the model and the experiment has been reached. This is usually done through the minimization of a quadratic objective function

$$F(\mathbb{C}) = \sum_{n} \left(\frac{f_n^{exp} - f_n^{cal}(\mathbb{C})}{f_n^{exp}} \right)^2, \tag{4}$$

where n is the number of measured frequencies. An issue of that approach is that it requires to correctly pair the measured frequencies f_n^{exp} to their calculated counterparts f_n^{cal}. If the initial guess is far from the actual elasticity and if the predicted resonant modes are not all observed experimentally, as it is the case for high damping materials such as bone, the correct pairing is difficult to obtain. Here, we used a Bayesian formulation of the inverse problem that automatically solves the joint problem of finding the correct pairing of frequencies and estimating the elastic properties. The Bayesian formulation was validated by comparing optimized elastic coefficients for several characteristic specimens with the traditional formulation (Bernard et al. 2013, 2014). A detailed presentation of the Bayesian approach is out of the scope of this paper. The method is explained in details in Bernard et al. (2015). Suffice it to say that it is a statistical approach which includes the modeling errors and the uncertainties on the measurement of resonant frequencies in the inverse problem. The solution is obtained in the form of a posterior probability density function of each stiffness coefficient of each sample. From the probability density function, which is not a normal distribution in general, the value with the highest probability was obtained (specimen elastic coefficient) together with the width of the 68 % confidence interval (measurement uncertainty).

2.4 Viscoelasticity measurements

The stiffness coefficients are obtained with RUS with the procedure described above without considering damping. Damping can be assessed a posteriori based on the width of the resonant peaks which is related to the quality factors Q_k of each mode defined in Eq. (3). Bone viscoelasticity was modeled by adding an imaginary part to the stiffness coefficients

$$C_{ij}^{*} = C_{ij} + iC'_{ij} = C_{ij}(1 + iQ_{ij}^{-1}), \tag{5}$$

where Q_{ij}^{-1} are the ratios of the imaginary (C'_{ij}) to the real (C_{ij}) part of the stiffness constants. Note that Q_{ij}^{-1} is the same physical quantity as $\tan(\delta)$, another popular way of reporting bone damping values (Lakes 2001), where δ is the phase shift between a harmonic loading and the mechanical response in a vibrational mechanical tests.

We take advantage of the fact that when the inverse damping ratios Q_{ij}^{-1} are small ($Q_{ij}^{-1} \ll 1$), they can be linearly related to the inverse of the peaks quality factors Q_k^{-1} (Leisure et al. 2004; Ogi et al. 2003; Bernard et al. 2014) by

$$Q_k^{-1} = \sum_{i,j} \frac{2C_{ij}}{f_k} \frac{\partial f_k}{\partial C_{ij}} Q_{ij}^{-1}. \tag{6}$$

The coefficients of this linear system are the normalized relative sensitivities of the resonant mode k to the elastic coefficients, i.e.,

$$\sum_{i,j} \frac{2C_{ij}}{f_k} \frac{\partial f_k}{\partial C_{ij}} = 1. \tag{7}$$

When the elastic constants C_{ij} have been estimated, Eq. (6) can be inverted to yield the damping ratios Q_{ij}^{-1} from the measured quality factors Q_k^{-1}. However, many quality factors Q_k are difficult to estimate precisely particularly when peak overlapping is strong as in the case of bone. Furthermore, the relative sensitivities of some frequencies to some elastic moduli are low, so that the inversion is badly conditioned and sensitive to errors in the measured Q_k.

Seven specimens were selected for an anisotropic analysis of the viscoelasticity. The criterion for selection of these specimens was that several resonant peaks were clearly marked and separated from the others and that those peaks could be unambiguously associated with their counterparts predicted by the model. For these specimens, the damping ratios were inverted using the analogous of Eq. (6) formulated for the engineering moduli. Since the sensitivity of the resonant frequencies to the imaginary part of the Poisson's ratio is small, the latter was neglected in the calculations. This reduces the number of unknowns to three, as the relation between the

transverse shear modulus C_{66}, Young's modulus E_1 and Poisson's ratio ν_{12}

$$C_{66} = \frac{E_1}{2(1+\nu_{12})} \tag{8}$$

entails the equality of the damping ratios Q_{66} and Q_{E_1} when ν_{12} is real. Then, the system of equations to solve is

$$Q_k^{-1} = \frac{2E_3}{f_k}\frac{\partial f_k}{\partial E_3}Q_{E_3}^{-1} + \frac{2E_1}{f_k}\frac{\partial f_k}{\partial E_1}Q_{E_1}^{-1} + \frac{2C_{44}}{f_k}\frac{\partial f_k}{\partial C_{44}}Q_{44}^{-1}, \tag{9}$$

with k (i.e., the number of resonant peaks included in the analysis) ranging from 7 to 9 depending on the specimen. As a matter of facts, the reduction to a three-parameters model drastically improves the conditioning of the inversion, even for a low number of measured peak width.

We also performed a simplified measurement of the viscoelasticity for all the specimens. The first vibration mode of RP specimens with small aspect ratios is usually a pure shear mode (Migliori and Sarrao 1997), because shear waves have a smaller velocity than longitudinal waves. Moreover, many of the specimens in that study are longer in direction 3 (axial direction of bone), so that the first resonant mode depends mainly on the axial shear modulus C_{44}. Hence, the mechanical quality factor of the first resonant mode Q_{first} can be directly related to the damping ratio Q_{44}. Eq. (6) then reduces to

$$Q_{first} \approx Q_{44}. \tag{10}$$

The quality of this approximation was checked by calculating the relative sensitivity of the first peak to the axial shear coefficient C_{44}, using the specimens dimensions and estimated stiffness. We found that the sensitivity is larger than 0.8 for the majority of the population. For the analysis, we discarded the samples for which the sensitivity was lower than 0.8. Because the frequency of the first peak spans a large range (100–400 kHz), it was questionable whether the width of the first resonant peak was dependent on its central frequency. This was, however, not the case (there was no correlation between central frequency and peak width, $p = 0.99$). Moreover, Q_{first} was not correlated with the relative sensitivity of the first peak to the axial shear stiffness C_{44} ($p = 0.64$).

2.5 Comparison with other studies

The elasticity–density relationships obtained in this study were compared with the results of former studies, which are described in Table 1. These studies all used ultrasound to measure either (i) stiffness coefficients C_{ij} based on the measurement of the travel time of longitudinal and shear plane waves along the different anatomical directions of RP samples (Rudy et al. 2011; Granke et al. 2011); or (ii) Young's modulus E_3 in the direction of the bone long axis based on the propagation of bar waves (Grimal et al. 2009) or the measurement of a longitudinal vibration mode in a long and thin sample (Haupert et al. 2014). In all these studies, the wet mass density was also reported. The data of Rudy et al. (2011) were available as supplementary online material, while the other studies have been conducted in the group of the first author. Note that since Rudy et al. (2011) and Granke et al. (2011) did not measure all the coefficients of the stiffness tensor, it was not possible to calculate the Young's moduli. The hypothesis that bone is transverse isotropic was not done a priori in Rudy et al. (2011) and Granke et al. (2011); for the purpose of comparison with the present work, we averaged for each specimen C_{11} and C_{22} values on the one hand and C_{44} and C_{55} values on the other hand.

Table 1 Description of cortical bone data sets for which elasticity–density relationships are compared

	Bone site	Quadrant	Number of specimens	Number of donors
This study (B)	Tibia mid-d.	A	55	19
Granke (G)	Femur mid-d.	L, M, P	21	10
Rudy (R)	Femur mid-d.	A, L, M, P	36*	9
Haupert (H)	Femur mid-d.	–	16	4
Grimal (G)	Four levels in the femur d.	A, L, M, P	68	3

Data from the present study, Granke et al. (2011), Rudy et al. (2011), Haupert et al. (2014) and Grimal et al. (2009) are referred in the figures with (B), (G) , (R), (H) and (G), respectively
d. diaphysis, *A* anterior, *L* lateral, *P* posterior, *M* medial
(*) shear coefficients C_{44} and C_{66} have been measured for a subset of 20 specimens

The elasticity–density relationships observed in the present study were compared to previously published empirical laws given in Table 2. We used the laws derived from measurements of human tibia specimen with mechanical (Snyder and Schneider 1991) and ultrasound (Rho et al. 1995) methods, in addition to the law of Carter and Hayes (1977).

3 Statistical analysis

Linear least squares regressions were conducted to analyze the relationships between the different elastic coefficients and between the elastic coefficients, or the quality factors, and mass density. The level of significance for all the tests was set to $p = 0.05$.

Table 2 Empirical laws from previous studies which are compared to the data of the present study

	Bone site	Law	Regression coefficient r^2 from the original study
Rho	Tibia	$E_3 = -3.842 + 0.013\,\rho$	0.53
Snyder(*)	Tibia	$E_3 = -23.5 + 0.022\,\rho$	0.55
Carter		$E_3 = 3.79(\rho\ 10^{-3})^3$	

Density (ρ) is in kg.m^{-3} and Young's modulus (E_3) is in GPa
Rho: Rho et al. (1995); Snyder: Snyder and Schneider (1991); Carter: Carter and Hayes (1977)
(*) Apparent mass density was obtained as the centrifuged weight of the wet sample divided by its volume

4 Results

Between 9 and 21 frequencies were obtained from the measured spectra for each specimen, with an average of 16 frequencies per specimen. Typical spectra for one specimen are shown in Fig. 2. The first resonant frequency of each specimen was in the range 100–400 kHz and the highest frequency in the range 200–1 MHz. Such a range of variation of the first frequency may be expected given the variability of specimens dimensions. For four specimens, the error (eq. 4) between measured and predicted frequencies was about 5 %, which is very high by the RUS standards. These specimens were excluded from all the subsequent analyses. For the other specimens, the error was about 1 %, which reflects the relative agreement between the predicted and measured frequencies. The median values of the relative half-width of the 68% confidence intervals were 7.3, 4.4, 10.9, 1.3 and 2.0 % for C_{11}, C_{33}, C_{13}, C_{44} and C_{66}, respectively, and 2.3, 2.8, 10.1, 7.6 and 8.4 % for E_1, E_3, ν_{12}, ν_{13} and ν_{31}, respectively.

Mean values, standard deviations and ranges of values of the measured quantities are reported in Table 3. The data are provided as electronic supplementary material (Online Resource 1). The measured mean values of the Poisson's ratios are compared to results of the literature in Table 4.

Except for two of the Poisson's ratios and for C_{13}, the correlations between the different stiffness coefficients were very high: larger than $r^2 = 0.70$ for all cases and larger than $r^2 = 0.85$ for most of the cases (Tables 5, 6). This is illustrated in Fig. 3 where C_{11}, C_{33}, C_{44}, E_1 and E_3 are plotted against the shear coefficient C_{66}.

Except for ν_{12}, all elastic coefficients and anisotropy ratios were significantly correlated with mass density (Table 7). Mass density variations explained about or more than 80 % of the variations of C_{11}, C_{33}, C_{44}, C_{66}, E_1 and E_3.

Longitudinal and shear stiffness coefficients of the present study and those of previous studies are plotted as a function of bone density in Figs. 4 and 5. Poisson's ratios as a function of bone density are plotted in Fig. 6. The axial Young's modulus E_3 is plotted in Fig. 7 together with the values of E_3 from previous studies and previously published empirical laws of elasticity as a function of density.

The anisotropy ratios as a function of density are plotted in Figs 8, 9, and 10.

Table 3 Mean, standard deviation (SD) and range of variation of the measured quantities.

	ρ	C_{11}	C_{33}	C_{13}	C_{44}	C_{66}	E_1	E_3	ν_{12}	ν_{13}	ν_{31}	Q_{44}
Mean	1879	14.79	26.64	8.31	5.52	3.65	10.25	20.28	0.4	0.19	0.39	28.68
SD	105	3.39	3.48	1.01	1.05	0.9	2.57	3.93	0.04	0.02	0.08	3.74
Min	1576	5.34	16.79	5.14	2.41	1.2	3.14	7.85	0.21	0.14	0.29	17.3
Max	2011	20.27	31.12	11.03	7.21	5.03	14.32	25.35	0.49	0.3	0.68	33.1

ρ is in kg.m^{-3}, elastic coefficients except Poisson's ratios are in GPa

Table 4 Mean Poisson's ratios measured in this study compared to values of the literature, measured using ultrasound wave velocities

	This study	Ashman et al. (1984)	Rho (1996)
Bone	Tibia	Femur	Tibia
Number of specimens	55	60	96
ν_{12}	$\nu_{12} = \nu_{21}$	0.376	0.420 (0.075)
ν_{21}	= 0.397 (0.042)	0.422	0.435 (0.057)
ν_{13}	$\nu_{13} = \nu_{23}$	0.222	0.237 (0.041)
ν_{23}	= 0.191 (0.024)	0.235	0.231 (0.035)
ν_{31}	$\nu_{31} = \nu_{32}$	0.371	0.417 (0.048)
ν_{32}	= 0.390 (0.077)	0.350	0.390 (0.021)

Standard deviations are indicated in parenthesis, if available. In all studies, direction 3 is the axial direction of bone. Our study assumes a transverse isotropic symmetry, which imposes equality of pairs of Poisson's ratios

Table 5 Squared Pearson's correlation coefficients r^2 between the stiffness coefficients

	C_{11}	C_{33}	C_{13}	C_{44}	C_{66}
C_{11}	1	**0.71**	0.68	**0.91**	**0.91**
C_{33}	**0.71**	1	0.45	**0.92**	**0.89**
C_{13}	0.68	0.45	1	0.61	0.54
C_{44}	**0.91**	**0.92**	0.61	1	**0.98**
C_{66}	**0.91**	**0.89**	0.54	**0.98**	1

All correlations reached the significance level. Coefficients larger than 0.70 are in bold face

Table 6 Squared Pearson's correlation coefficients r^2 between the engineering moduli.

	E_1	E_3	ν_{12}	ν_{13}	ν_{31}	C_{44}	C_{66}	Q_{44}
E_1	1	**0.84**	0.20	0.27	**0.84**	**0.97**	**0.99**	**0.73**
E_3	**0.84**	1	0.08	0.52	**0.76**	**0.87**	**0.87**	**0.70**
ν_{12}	0.20	0.08	1	0.22	0.42	0.12	0.12	–
ν_{13}	0.27	0.52	0.22	1	0.51	0.23	0.27	0.09
ν_{31}	**0.84**	**0.76**	0.42	0.51	1	**0.76**	**0.79**	0.46
C_{44}	**0.97**	**0.87**	0.12	0.23	**0.76**	1	**0.98**	**0.79**
C_{66}	**0.99**	**0.87**	0.12	0.27	**0.79**	**0.98**	1	**0.77**
Q_{44}	**0.73**	**0.70**	–	0.09	0.46	**0.79**	**0.77**	1

All correlations reached the significance level. Coefficients larger than 0.70 are in bold face

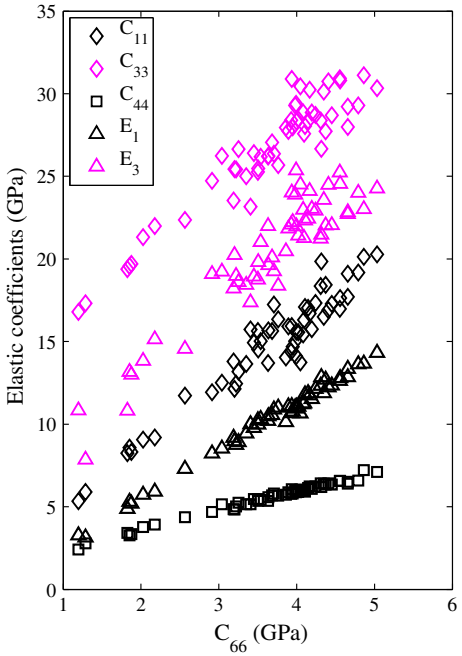

Fig. 3 Stiffness and engineering coefficients values as a function of C_{66} values

The damping ratio of the axial shear coefficient is plotted in Fig. 11 as a function of density for 49 specimens for which the first peak was sufficiently sensitive to Q_{44}.

Table 7 Results of the linear correlation analyses of the elastic coefficients and engineering moduli (GPa, except Poisson's ratios), viscoelastic parameter Q_{44} (no dimension) and anisotropy ratios (no dimension) versus the mass density (g/cm^{-3}). All reported coefficients are significant

Parameter	Corr. coef. r^2	Slope	Intercept
C_{11}	0.79	28.8	−39.3
C_{33}	0.85	30.6	−30.9
C_{13}	0.52	6.9	−4.7
C_{44}	0.89	9.4	−12.2
C_{66}	0.87	8.0	−11.3
E_1	0.85	22.6	−32.3
E_3	0.80	33.5	−42.7
ν_{12}	0.09	–	–
ν_{13}	0.23	−0.11	0.40
ν_{31}	0.71	−0.61	1.54
C_{33}/C_{11}	0.59	−2.5	6.57
C_{44}/C_{66}	0.76	−1.31	4
E_3/E_1	0.53	−2.02	5.84
Q_{44}	0.72	31.3	−30.4

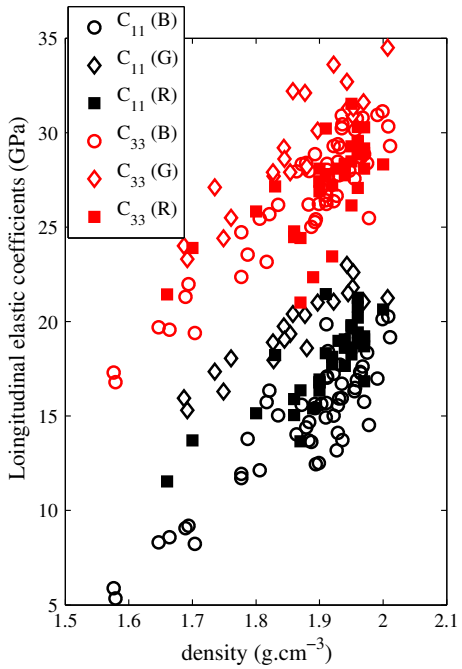

Fig. 4 Comparison of C_{33} and C_{11} from different studies (Table 1): present study (B), Granke et al. (G), Rudy et al. (R)

The results of the anisotropic viscoelastic analysis for seven selected specimens are presented in Fig. 12. The coefficients were calculated based on 7 to 9 peak widths. The predicted peaks width using the determined complex stiffness tensor agreed with measurement within 5 % in average, which is comparable to the precision of the measurement of the peak width. Despite the somewhat large uncertainties on the

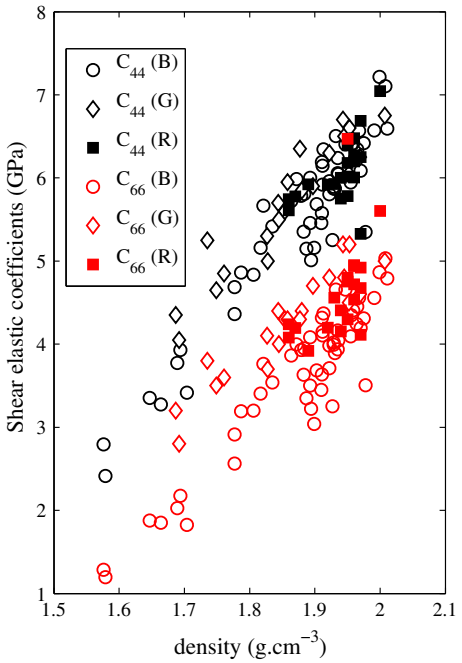

Fig. 5 Comparison of C_{11} and C_{66} from different studies (Table 1): present study (B), Granke et al. (G), Rudy et al. (R)

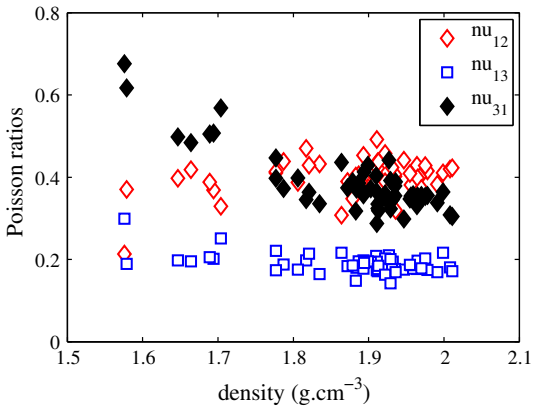

Fig. 6 Poisson's ratios as a function of mass density

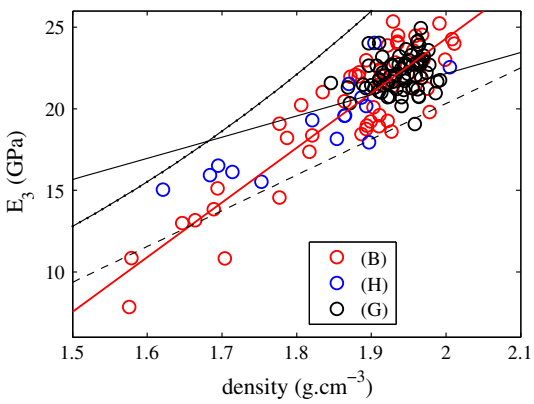

Fig. 7 Comparison of E_3 from different studies (Table 1) and empirical laws (Table 2); '—' Rho; '---' Carter; '- -' Snyder; present study (B, regression *line in red*); Haupert et al. (H); Grimal et al. (G)

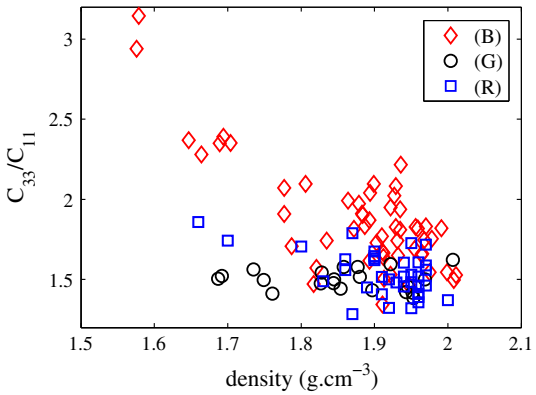

Fig. 8 Comparison anisotropy ratio C_{33}/C_{11} from different studies. B: present study; G: Granke et al.; R: Rudy et al.

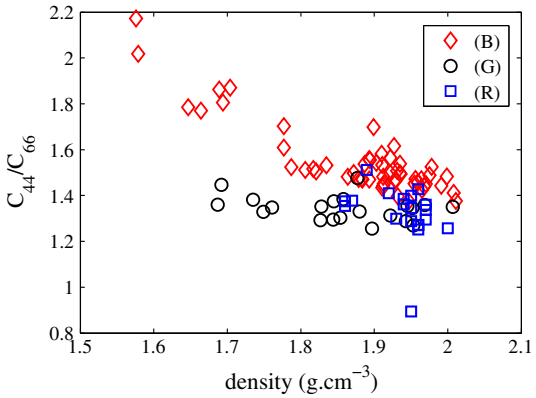

Fig. 9 Comparison anisotropy ratio C_{44}/C_{66} from different studies. B: present study; G: Granke et al.; R: Rudy et al.

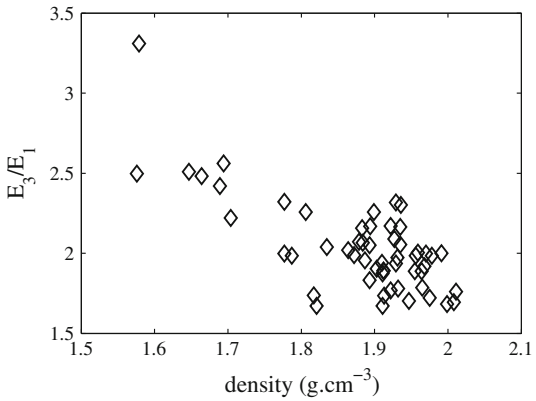

Fig. 10 Anisotropy ratio E_3/E_1 as a function of bone mass density

results, anisotropy of the damping ratios can be observed: $Q_{E_3}^{-1} < Q_{44}^{-1} < Q_{E_1}^{-1} = Q_{66}^{-1}$, i.e., the damping is weaker in axial direction of bone, both for Young's and shear moduli. Adding the Poisson's ratios in the analysis did not significantly improve the agreement (result not shown).

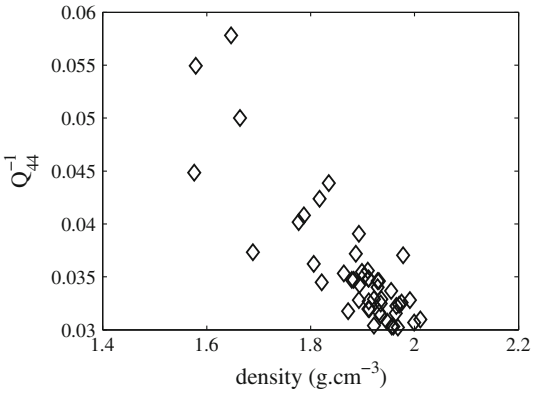

Fig. 11 Damping factor of the first resonant peak, approximately equal to the axial shear damping ratio Q_{44}, as a function of bone mass density

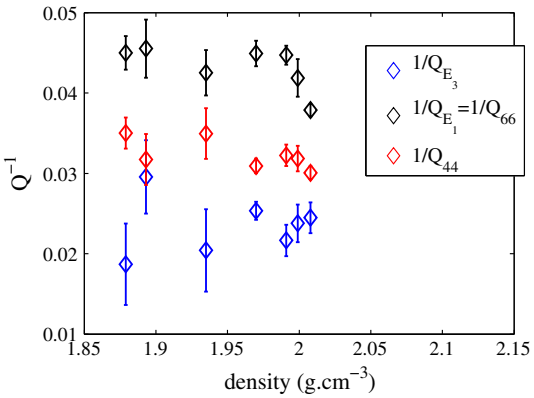

Fig. 12 Anisotropic viscoelastic coefficients for seven selected specimens

5 discussion

This study aimed at quantifying, by means of RUS, the mesoscale elastic and viscoelastic properties of human tibial cortical bone and relate these to density.

The precision of the mesoscale elastic coefficients was found to be 1–2 % for the shear coefficients and 2–3 % for the Young's moduli (median values), while the other coefficients are determined with a slightly lower precision. This ordering of the precision values is due to the variable relative sensitivity of RUS to these different coefficients (Migliori and Sarrao 1997; Landa et al. 2009). Better precision can be achieved with RUS when more resonant peaks can be measured for each specimen, which is in general difficult for bone due to high damping. In RUS, the value of the root mean square (RMS) error (Eq. 4) between measured and predicted frequencies is an indication of the quality of the measurement. Here, the median RMS value was 0.83 %, which indicates a somewhat lower precision compared to that we obtained previously for a bone specimen (0.3 %) (Bernard et al. 2013) or for two bone mimetic material specimens (0.42 and 0.45 %) (Bernard et al. 2014). In general, the misfit between predicted and measured frequencies has several potential causes: (1) The geometry of the specimens may differ from a perfect rectangular parallelepiped. Deviations from perpendicularity of about 1° or larger can shift the frequencies of a few tenth of percents (Migliori and Sarrao 1997). (2) The signal processing consisting in fitting Eq. (3) to obtain experimental frequencies is known to be a user-dependent step; in particular, one or a few frequencies may be missed, which increases the error. (3) The hypothesis that cortical bone is transverse isotropic is only true to a certain extent. While previous authors (Espinoza Orías et al. 2009; Granke et al. 2011) found weak or nonexistent statistical differences in elastic properties in the plane transverse to the bone axis at the femur mid-diaphysis, some anisotropy may still occur for individual specimens, for example, caused by a gradient in density between the inner an outer parts of the cortical shell. (4) The method as implemented assumes that the orthogonal reference frame defined by the specimen faces corresponds to the principal directions of the anisotropic bone material. Granke et al. (2015) estimated that a deviation of 10° between the assumed and actual material symmetry axis could results in an error of less than 2 % on the stiffness coefficients estimated from time-of-flight measurements. (5) The model of vibrating specimen assumes homogeneity of the material, while bone is heterogeneous. RUS has been shown to be weakly sensitive to small linear gradients of elastic properties (Seiner et al. 2012). Also, the effect of a localized mass perturbation (e.g., a large pore in bone) was found to be associated with frequency shifts up to 0.2 % (Ulrich et al. 2002).

The inverse problem solved when using RUS requires to provide a priori information on the measured specimen since the solution of the fit Eq. (4) may not be unique. When the inverse problem is solved in a Bayesian framework, the a priori information consists in reasonable mean values of each unknown coefficient and a reasonable covariance matrix which describes a statistical relationship between the different coefficients. In the specific Bayesian approach used here, this a priori information is not fixed before solving the inverse problem but is itself an unknown. This is known as hierarchical Bayes modeling (Gelman et al. 2013). The data of all the specimens are processed together to converge toward the solution for each specimen regularized by the statistical properties of the group of samples. This approach was chosen because it is robust and is deeply rooted in the hypothesized physical properties of bone. Indeed, because the specimens were taken from the same anatomical region of the tibia of aged donors, their properties are expected to belong to a simple statistical distribution. The method may introduce a slight bias in the correlations obtained between the different elastic coefficients. Although there is no direct means to test whether this bias exists, we feel that the bias is unlikely significant based on preliminary tests that we did for several specimens.

Most of the elastic coefficients were highly correlated. For instance, we found $r^2 = 0.71$ between C_{11} and C_{33} and $r^2 = 0.98$ between C_{44} and C_{66}. This is in line with the data published in previous studies, e.g., from the data of Granke et al. (2011), the corresponding correlation coefficients can be calculated: $r^2 = 0.83$ between C_{11} and C_{33} and $r^2 = 0.93$ between C_{44} and C_{66}. From the data of Rudy et al. (2011), the corresponding correlation coefficients can be calculated: $r^2 = 0.54$ between C_{11} and C_{33} and $r^2 = 0.20$ between C_{44} and C_{66}; however, the range of specimens' density was somewhat smaller in that study compared with the present study. Dong and Guo (2004) found weaker or nonsignificant correlations, but the different coefficients, obtained with traditional mechanical methods, were not measured on the same specimens. In the present study, we obtained high correlation coefficients likely because (1) RUS is in general a more precise measurement method than traditional mechanical methods or than the measurement of ultrasound time-of-flight (Migliori and Sarrao 1997); (2) all our specimens were taken from a relatively limited anatomical region in the medial quadrant of the mid-diaphysis; and (3) the range of density is somewhat larger than in some other similar studies. The strength of these correlations strongly suggests that there is a relatively simple relationship between the variations of, on the one hand, microstructural and compositional features at small scales and, on the other hand, the variations of mesoscale properties. We observed that, to a large extent, the variations of all the coefficients can be written as a function of one single coefficient (as illustrated for C_{66} in Fig. 3). The properties at the mesoscale being entirely determined by microscale features and composition, our data shed light on the possible variations of these features in the different specimens.

The above observation suggests that essentially only one microscale property changes between the different specimens (e.g., porosity) or several microscale properties change, but in a 'coordinated' (i.e., non-independent) manner. Simple homogenization models of cortical bone assuming a bone matrix with fixed properties and a cylindrical porosity of variable volume fraction (Granke et al. 2011; Parnell et al. 2012; Hellmich et al. 2008) are consistent with this observation. However, there are evidences that the variation of elastic coefficients is not only due to the varying porosity only but also to variations of the stiffness of the bone matrix (Rho et al. 2002; Granke et al. 2011; Rohrbach et al. 2015). The bone matrix should be less stiff (younger) and more porous when remodeling is more intense and stiffer and less porous when remodeling is less intense. Such a coupled evolution of matrix properties and porosity is consistent with our observation that all mesoscale coefficients are highly correlated.

The values of elasticity from the present study were shown to be overall highly consistent with the data of four previous studies (Figs. 4, 5, 7). This is noteworthy because: (1) the different data sets were obtained with different methods and by different investigators; (2) our data are only for the medial quadrant of the mid-diaphysis of the tibia, while others are for different regions in the femur diaphysis. Also, the empirical relationships derived previously globally fits with our data, especially that of Snyder and Schneider (1991) (Fig. 7).

All the elastic coefficients, engineering moduli and anisotropy ratios showed a statistically significant correlation with the mass density (Table 7). This dependence is strong ($r^2 > 0.5$), except for ν_{12} and ν_{13} which appear to be almost independent of density. The elastic coefficients C_{ij} and the Young's moduli increase as a function of mass density, while the Poisson's ratios and the anisotropy ratios decrease with mass density. Mass density is indeed known to be a good predictor of bone millimeter-scale stiffness, both for trabecular (Carter and Hayes 1977) and cortical tissues (Schaffler and Burr 1988; Keller 1994). Linear or power law relations between density and stiffness are used in studies of bone mechanics at the organ scale to set the stiffness in the numerical models from density measurement (Schileo et al. 2007, 2008; Austman et al. 2008). Measuring femoral bone elasticity using ultrasound waves, Espinoza Orías et al. (2009) also observed correlations between mass density and longitudinal stiffness with similar strength, but no correlation with shear stiffness.

The observed decrease in longitudinal stiffness anisotropy ratio C_{33}/C_{11} with increasing density is also consistent with the findings of Espinoza Orías et al. (2009), who reported a slope of -2.95 ($r^2 = 0.61$), close to our results (Table 7; Fig. 8). Moreover, micro-mechanical models typically predict an increase in the anisotropy with increasing vascular porosity (e.g., Parnell and Grimal 2009; Parnell et al. 2012). If mineralized matrix properties are assumed to be fixed, density and porosity are inversely related, which is consistent with the observed variation in anisotropy. Note that the longitudinal stiffness anisotropy ratios C_{33}/C_{11} reported here are larger than previously measured or predicted values for femoral bone: Espinoza Orías et al. (2009) found C_{33}/C_{11} in the range 1.25–1.75, and Parnell et al. (2012) predicted 1.3–1.5 for the physiological range of porosity. We observe a larger range of 1.35–3.15. This might partly be due to the large range of mass densities in our collection of specimens. Overall, the increase in anisotropy with decreasing density indicates that the transverse elastic properties (C_{11}, E_1 and C_{66}) are more sensitive than the axial properties (C_{33}, E_3 and C_{44}) to changes in mass density.

Two of the Poisson's ratios—ν_{12} and ν_{13}—were found to vary weakly with density (Table 7; Fig. 6). This is consistent with the model of Parnell et al. (2012), which predicts small variations in Poisson's ratios as a function of porosity. The mean values are $\nu_{12} = 0.397$ and $\nu_{13} = 0.191$, in good agreement with values previously measured on femur and

tibia using ultrasound wave velocities (Table 4). The third Poisson's ratio ν_{31} is related to ν_{13} through $\frac{\nu_{31}}{E_3} = \frac{\nu_{13}}{E_1}$; therefore, the observed variations of ν_{31} with density reflect the variation of the anisotropy ratio E_3/E_1.

We found a strong correlation ($r^2 = 0.72$, Fig. 11) between shear damping in the direction of the bone long axis and mass density. Damping increases as the mass density decreases. The relationship between mass density and intrinsic damping has not been reported before as far as we know. Furthermore, the anisotropy of the viscoelastic shear and Young's moduli (Fig. 12) was evidenced from seven selected specimens corresponding to a limited density range. Such an anisotropic viscoelasticity for the Young's modulus has been previously observed in bovine cortical bone using mechanical tests (Iyo et al. 2004). In general, damping values depend on the measurement frequency (Garner et al. 2000). Here, damping coefficients are measured in the range 100–400 kHz. More precisely, a unique value is obtained for the entire range according to the principle of RUS which assumes a frequency-independent behavior in the measurement frequency range. It is not clear which physical phenomena are responsible for the viscoelastic behavior of bone (Lakes and Katz 1979; Lakes 2001), particularly at ultrasonic frequencies. Among several potential causes, we can mention fluid motions inside the pores, thermomechanical effects and motions at interfaces (e.g., motion of at the cement lines between osteons or motion of the collagen lamellae inside osteons). Due to the structural anisotropy of cortical bone, all these phenomena are expected to entail an anisotropic viscoelastic behavior. As a mechanism of energy dissipation, viscoelasticity is intimately related to crack initiation and propagation in bone (Schapery 1975; Ritchie et al. 2009), and bone strength and toughness have been found to be rate dependent (Carter and Hayes 1977; Currey 1988). Viscoelasticity could also be a marker of tissue quality related to the properties of the collagen–mineral compound (Les et al. 2004; Yang et al. 2013). In the present study, RUS is shown to be a convenient method to measure energy dissipation in bone; in particular Q_{44}. The agreement between measured peak widths and peak widths predicted from Eq. (3) after solving the RUS inverse problem was about 5 %, which is comparable to the precision of the measurement and comparable to results reported previously for similar analyses on low damping materials (Seiner et al. 2013). In contrast, bone viscoelasticity is difficult to characterize using ultrasound methods based on wave propagation, because these methods cannot usually separate two cumulative effects of energy losses: intrinsic viscoelastic losses and scattering effects (Lakes et al. 1986; Haïat 2011).

One limitation of this study is that the measurement of anisotropic viscoelasticity could not be done for all specimens. As discussed in the paper, such a measurement requires that a sufficient number of the resonant peaks are well separated from each other. This is required for their width to be accurately estimated. Note, however, that it should be possible to design the shape of the specimens specifically for anisotropic viscoelasticity measurements to achieve a good peak separation.

6 Conclusion

This paper presents a set of data to discuss elasticity–density relationships which is unique for two reasons: (i) all the elastic coefficients of 55 bone specimens were measured with RUS, which is more accurate than traditional ultrasound or mechanical techniques; and (ii) specimens were all prepared from a limited anatomical region (the antero-medial part of the mid-tibia).

In this study, we reported: (1) strong statistical relationships between most of the elastic coefficients and (2) strong elasticity–density relationships at the mid-tibia. The considered elastic coefficients are all the engineering moduli and all the stiffness coefficients which completely describe a transverse isotropic material. The relationships should be useful to design or update procedures to allocate cortical bone anisotropic properties in organ-scale bone models using Hounsfield values from computed tomography scans as a surrogate for mass density.

Our results are in line with some previous studies which had evidenced a strong relationship between some of the elastic coefficients and mass density but is original because of a unique anatomical origin of the specimens, which implies that all specimen have likely been subjected to similar strain histories.

This study has also introduced RUS as a convenient and accurate method to measure large series of bone specimens. The RUS setup is simple and relatively inexpensive. The measurements themselves do not require specific ultrasound skills. However, at the present stage of the development of the method, the processing of the resonance spectrums requires the intervention of a user with signal processing skills. The derivation of stiffness coefficients based on resonance frequencies (i.e., the minimization of Eq. (4)) has been automatized.

Many multiscale cortical bone models have been proposed to derive mesoscale elastic properties based on a more or less large number of parameters (e.g., Crolet et al. 1993; Hellmich and Ulm 2004; Dong and Guo 2006; Deuerling et al. 2009; Grimal et al. 2011). These parameters describe the composition and the microstructure (collagen or mineral orientation, osteon size, relative volumes of osteonal and interstitial tissues, types of porosities, etc.) at different scales below the millimeter scale. Our data suggest that relatively simple multiscale models of cortical bone elastic properties could be

accurate provided that one or a few parameters are well chosen to account for the mesoscale changes.

The mid-tibia is an important site for the in vivo assessment of bone status with ultrasound techniques. The strong relationships evidenced at this site between the different elastic coefficients have important consequences for the processing of ultrasound data obtained with guided waves techniques. The latter processing consists of an inverse problem which aims at determining simultaneously bone thickness and elasticity (both determinants of guided waves properties). This study provides unique a priori information to solve this inverse problem.

Acknowledgments This work has been conducted within the European Associated Laboratory 'Ultrasound Based Assessment of Bone' (ULAB), a cooperation of centers in Paris (France) and Kiel and Berlin (Germany), funded by CNRS (France). This work was funded by the Agence Nationale pour la Recherche under a Grant No. ANR-13-BS09-0006-01, the Elsbeth-Bonhoff foundation, project ♯36 'Verbesserung der Abschätzung der Knochenbruchfestigkeit am proximalen Femur durch multitimodale Bestimmung von festigkeitsrelevanten Knochenmaterialeigenschaften' and was supported by the Deutsche Forschungsgemeinschaft (SPP 1420 grant Ra1380/7-3, Ra1380/9-1). JS is grateful for the support from the BSRT. We acknowledge Robert Wendlandt from UKSH Lübeck for the collection of the samples.

Conflict of interest The authors declare that they have no conflict of interest.

References

Ashman RB, Cowin SC, van Buskirk WC, Rice JC (1984) A continuous wave technique for the measurement of the elastic properties of cortical bone. J Biomech 17(5):349–361

Austman RL, Milner JS, Holdsworth DW, Dunning CE (2008) The effect of the density-modulus relationship selected to apply material properties in a finite element model of long bone. J Biomech 41(15):3171–3176

Bernard S, Grimal Q, Laugier P (2013) Accurate measurement of cortical bone elasticity tensor with resonant ultrasound spectroscopy. J Mech Behav Biomed Mater 18:12–19

Bernard S, Grimal Q, Laugier P (2014) Resonant ultrasound spectroscopy for viscoelastic characterization of anisotropic attenuative solid materials. J Acoust Soc Am 135(5):2601–2613

Bernard S, Marrelec G, Laugier P, Grimal Q (2015) Bayesian normal modes identification and estimation of elastic coefficients in resonant ultrasound spectroscopy. Inverse Probl. doi:10.1088/0266-5611/31/6/065010

Carter D, Hayes W (1977) The compressive behavior of bone as a two-phase porous structure. J Bone Joint Surg 59(7):954–962

Crolet JM, Aoubiza B, Meunier A (1993) Compact bone: numerical simulation of mechanical characteristics. J Biomech 26(6):677–687

Currey JD (1988) Strain rate and mineral content in fracture models of bone. J Orthop Res 6(1):32–38

Deuerling JM, Yue WM, Orias AAE, Roeder RK (2009) Specimen-specific multi-scale model for the anisotropic elastic constants of human cortical bone. J Biomech 42(13):2061–2067

Dong NX, Guo EX (2004) The dependence of transversely isotropic elasticity of human femoral cortical bone on porosity. J Biomech 37(8):1281–1287

Dong XN, Guo XE (2006) Prediction of cortical bone elastic constants by a two-level micromechanical model using a generalized self-consistent method. J Biomech Eng Trans ASME 128(3):309–316

Espinoza Orías AA, Deuerling J, Landrigan M, Renaud J, Roeder R (2009) Anatomic variation in the elastic anisotropy of cortical bone tissue in the human femur. J Mech Behav Biomed Mater 2(3):255–263

Foiret J, Minonzio JG, Chappard C, Talmant M, Laugier P (2014) Combined estimation of thickness and velocities using ultrasound guided waves: a pioneering study on in vitro cortical bone samples. IEEE Trans Ultrason Ferroelectr Freq Control 61(9):1478–1488

Foldes A, Rimon A, Keinan D, Popovtzer M (1995) Quantitative ultrasound of the tibia: a novel approach for assessment of bone status. Bone 17(4):363–367

Garner E, Lakes R, Lee T, Swan C, Brand R (2000) Viscoelastic dissipation in compact bone: implications for stress-induced fluid flow in bone. J Biomech Eng 122(2):166–172

Gelman A, Carlin JB, Stern HS, Dunson DB, Vehtari A, Rubin DB (2013) Bayesian data analysis, 3rd edn. CRC Press, Boca Raton

Granke M, Grimal Q, Saïed A, Nauleau P, Peyrin F, Laugier P (2011) Change in porosity is the major determinant of the variation of cortical bone elasticity at the millimeter scale in aged women. Bone 49(5):1020–1026

Granke M, Grimal Q, Parnell WJ, Raum K, Gerisch A, Peyrin F, Saïed A, Laugier P (2015) To what extent can cortical bone millimeter scale elasticity be predicted by a two phase composite model with variable porosity? Acta Biomater 12:207–215

Grimal Q, Haupert S, Mitton D, Vastel L, Laugier P (2009) Assessment of cortical bone elasticity and strength: mechanical testing and ultrasound provide complementary data. Med Eng Phys 31(9):1140–1147

Grimal Q, Raum K, Gerisch A, Laugier P (2011) A determination of the minimum sizes of representative volume elements for the prediction of cortical bone elastic properties. Biomech Model Mechanobiol 10(6):925–937

Grimal Q, Rus G, Parnell WJ, Laugier P (2011) A two-parameter model of the effective elastic tensor for cortical bone. J Biomech 44(8):1621–1625

Haïat G (2011) Linear ultrasonic properties of cortical bone: in vitro studies. In: laugier P, Haïat G (eds) Bone Quantitative Ultrasound. Springer, Berlin

Haupert S, Guérard S, Peyrin F, Mitton D, Laugier P (2014) Non destructive characterization of cortical bone micro-damage by nonlinear resonant ultrasound spectroscopy. PLoS One 9(1):e83599

Helgason B, Perilli E, Schileo E, Taddei F, Brynjolfsson S, Viceconti M (2008) Mathematical relationships between bone density and mechanical properties: a literature review. Clin Biomech 23(2):135–146

Hellmich C, Kober C, Erdmann B (2008) Micromechanics-based conversion of ct data into anisotropic elasticity tensors, applied to fe simulations of a mandible. Ann Biomed Eng 36(1):108–122

Hellmich C, Ulm FJ (2004) Can the diverse elastic properties of trabecular and cortical bone be attributed to only a few tissue-independent phase properties and their interactions? Biomech Model Mechanobiol 2:219–238

Iyo T, Maki Y, Sasaki N, Nakata M (2004) Anisotropic viscoelastic properties of cortical bone. J Biomech 37(9):1433–1437 0021–9290

Keller TS (1994) Predicting the compressive mechanical behavior of bone. J Biomech 27(9):1159–1168

Lakes R, Yoon HS, Katz JL (1986) Ultrasonic wave propagation and attenuation in wet bone. J Biomed Eng 8(2):143–148

Lakes RS (2001) Bone mechanics handbook, chap. Viscoelastic properties of cortical bone. CRC Press, Boca Raton

Lakes RS, Katz JL (1979) Viscoelastic properties of wet cortical bone—II. Relaxation mechanisms. J Biomech 12(9):679–687

Lakshmanan S, Bodi A, Raum K (2007) Assessment of anisotropic tissue elasticity of cortical bone from high-resolution, angular acoustic measurements. IEEE Trans Ultrason Ferroelectr Freq Control 54(8):1560–1570

Landa M, Sedlák P, Seiner H, Heller L, Bicanová L, Šittner P, Novák V (2009) Modal resonant ultrasound spectroscopy for ferroelastics. Appl Phys A 96:557–567

Lebedev AV (2002) Method of linear prediction in the ultrasonic spectroscopy of rock. Acoust Phys 48(3):339–346

Leisure R, Foster K, Hightower J, Agosta D (2004) Internal friction studies by resonant ultrasound spectroscopy. Mater Sci Eng A 370:34–40

Les CM, Spence CA, Vance JL, Christopherson GT, Patel B, Turner AS, Divine GW, Fyhrie DP (2004) Determinants of ovine compact bone viscoelastic properties: effects of architecture, mineralization, and remodeling. Bone 35(3):729–738

Migliori A, Sarrao J (1997) Resonant ultrasound spectroscopy. Wiley, New York

Ogi H, Nakamura N, Sato K, Hirao M, Uda S (2003) Elastic, anelastic, and piezoelectric coefficients of langasite: resonance ultrasound spectroscopy with laser-doppler interferometry. IEEE Trans Ultrason Ferroelectr Freq Control 50(5):553–560

Parnell WJ, Vu MB, Grimal Q, Naili S (2012) Analytical methods to determine the effective mesoscopic and macroscopic elastic properties of cortical bone. Biomech Model Mechanobiol 11:883–901

Parnell WJ, Grimal Q (2009) The influence of mesoscale porosity on cortical bone anisotropy. investigations via asymptotic homogenization. J R Soc Interface 6(30):97–109

Preininger B, Checa S, Molnar FL, Fratzl P, Duda GN, Raum K (2011) Spatial–temporal mapping of bone structural and elastic properties in a sheep model following osteotomy. Ultrasound Med Biol 37(3):474–483

Prevrhal S, Fuerst T, Fan B, Njeh C, Hans D, Uffmann M, Srivastav S, Genant HK (2001) Quantitative ultrasound of the tibia depends on both cortical density and thickness. Osteoporos Int 12(1):28–34

Raum K (2008) Microelastic imaging of bone. IEEE Trans Ultrason Ferroelectr Freq Control 55(7):1417–1431

Rho JY, Hobatho MC, Ashman RB (1995) Relations of mechanical properties to density and ct numbers in human bone. Med Eng Phys 17(5):347–355

Rho JY (1996) An ultrasonic method for measuring the elastic properties of human tibial cortical and cancellous bone. Ultrasonics 34(8):777–783

Rho JY, Zioupos P, Currey JD, Pharr GM (2002) Microstructural elasticity and regional heterogeneity in human femoral bone of various ages examined by nano-indentation. J Biomech 35(2):189–198

Ritchie RO, Buehler MJ, Hansma P (2009) Plasticity and toughness in bone. Phys Today 62(6):41–47

Rohrbach D, Lakshmanan S, Peyrin F, Langer M, Gerisch A, Grimal Q, Laugier P, Raum K (2012) Spatial distribution of tissue level properties in a human femoral cortical bone. J Biomech 45(13):2264–2270

Rohrbach D, Grimal Q, Varga P, Peyrin F, Langer M, Laugier P, Raum K (2015) Distribution of mesoscale elastic properties and mass density in the human femoral shaft. Connect Tissue Res 56(2): 120–132

Rudy DJ, Deuerling JM, Orías AAE, Roeder RK (2011) Anatomic variation in the elastic inhomogeneity and anisotropy of human femoral cortical bone tissue is consistent across multiple donors. J Biomech 44(9):1817–1820

Schaffler M, Burr DB (1988) Stiffness of compact bone: effects of porosity and density. J Biomech 21(1):13–16

Schapery R (1975) A theory of crack initiation and growth in viscoelastic media. Int J Fract 11(1):141–159

Schileo E, Taddei F, Malandrino A, Cristofolini L, Viceconti M (2007) Subject-specific finite element models can accurately predict strain levels in long bones. J Biomech 40(13):2982–2989

Schileo E, Dall'Ara E, Taddei F, Malandrino A, Schotkamp T, Baleani M, Viceconti M (2008) An accurate estimation of bone density improves the accuracy of subject-specific finite element models. J Biomech 41(11):2483–2491

Seiner H, Sedlak P, Bodnarova L, Kruisova A, Landa M, de Pablos A, Belmonte M (2012) Sensitivity of the resonant ultrasound spectroscopy to weak gradients of elastic properties. J Acoust Soc Am 131(5):3775–3785

Seiner H, Sedlák P, Koller M, Landa M, Ramírez C, Osendi M, Belmonte M (2013) Anisotropic elastic moduli and internal friction of graphene nanoplatelets/silicon nitride composites. Compos Sci Technol 75:93–97

Sievänen H, Cheng S, Ollikainen S, Uusi-Rasi K (2001) Ultrasound velocity and cortical bone characteristics in vivo. Osteoporos Int 12(5):399–405

Snyder SM, Schneider E (1991) Estimation of mechanical properties of cortical bone by computed tomography. J Orthop Res 9(3): 422–431

Talmant M, Foiret J, Minonzio JG (2010) Bone Quantitative ultrasound, chap. Guided Waves in Cortical Bone. Springer, New York

Ulrich TJ, McCall KR, Guyer RA (2002) Determination of elastic moduli of rock samples using resonant ultrasound spectroscopy. J Acoust Soc Am 111(4):1667–1674

Yang X, Muthukumaran P, DasDe S, Teoh SH, Choi H, Lim SK, Lee T (2013) Positive alterations of viscoelastic and geometric properties in ovariectomized rat femurs with concurrent administration of ibandronate and PTH. Bone 52(1):308–317

Zebaze RMD, Ghasem-Zadeh A, Bohte A, Iuliano-Burns S, Mirams M, Price RI, Mackie EJ, Seeman E (2010) Intracortical remodelling and porosity in the distal radius and post-mortem femurs of women: a cross-sectional study. Lancet 375(9727):1729–1736